CARBON 61 (2013) 507–514

Available at www.sciencedirect.com

SciVerse ScienceDirect

journal homepage: www.elsevier.com/locate/carbon

Correlation between topographic structures and local field emission characteristics of graphene-sheet films

Jiale Du [a], *Yu Zhang* [a], *Shaozhi Deng* [a,*], *Ningsheng Xu* [a], *Zhiming Xiao* [a], *Juncong She* [a], *Zhongshuai Wu* [b], *Huiming Cheng* [b]

[a] *State Key Laboratory of Optoelectronic Materials and Technologies, Guangdong Province Key Laboratory of Display Material and Technology, School of Physics and Engineering, Sun Yat-Sen University, Guangzhou 510275, People's Republic of China*

[b] *Shenyang National Laboratory for Materials Science, Institute of Metal Research, Chinese Academy of Sciences, Shenyang 110016, People's Republic of China*

ARTICLE INFO

Article history:
Received 14 March 2013
Accepted 2 May 2013
Available online 23 May 2013

ABSTRACT

In an early report, some of us have demonstrated that graphene-sheet films prepared by electrophoretic deposition (EPD) method have great potential as high-performance field emission cathode. We report that the field emission performance from such graphene-sheet films may be enhanced. We have investigated the correlation between topographic structures and local field emission characteristics of graphene-sheet films, prepared with changing EPD deposition time. Detailed experiments show that samples prepared with longer deposition time have better field emission performance. Both scanning electron microscopy and high resolution transmission electron microscopy images show that the topographic structure of the surface layer of the samples deposited with longer time is formed with higher density of graphene sheets with shorter length and fewer graphene layers, in comparison with those with shorter deposition times. Such topographic structure is found experimentally to give large field enhancement. Computer simulation further confirms that a thinner graphene sheet will give more significant geometrical field enhancement at the corner of graphene sheet. Theoretical analysis shows that in an EPD process, longer-length graphene sheets will be deposited before shorter ones, explaining why with longer deposition time, the topographic structure of surface layer consists of shorter-length graphene sheets.

1. Introduction

Graphene [1–3], one may consider as an isolated atomic plane of graphite, has received worldwide attention since its discovery. Graphene and graphene-based films have been shown to have outstanding field emission properties due to its high aspect ratio, excellent electrical property, and stable physical and chemical properties. Most of the studies are mainly focused on the macro-field emission behavior of a large number of graphene sheets, including a group of single-layer graphene and multi-layer graphene (MLG). For example, Wu et al., some of our authors, have established a process to prepare graphene-sheet films, and have demonstrated their excellent field emission properties [4,5]. The field emission properties of single-layer graphene films [5], vertically aligned few-layer graphene (FLG) sheets [6–8], multi-layer graphene films [9,10],

* *Corresponding author.*
E-mail address: stsdsz@mail.sysu.edu.cn (S. Deng).
0008-6223/$ - see front matter
http://dx.doi.org/10.1016/j.carbon.2013.05.031

graphene aggregated films [11], and graphene-based composite/hybrid films [12–14] have also been shown to be comparable or even better to other carbon nanomaterials, such as carbon nanotube (CNT), in terms of low emission threshold field and high emission current density. Many authors have also investigated their potential applications in flexible and transparent field emission devices [15,16]. Furthermore, some studies have also been carried out to look into the fundamental behaviors and the underlying physics of field emission of single-layer graphene. Lee et al. investigated the field emission behavior of planar graphene layers using a nanomanipulator inside a scanning electron microscope (SEM) [17]. Wang et al. created a nanogap with atomically parallel edges of single-layer graphene and studied the field emission characteristics [18]. Xiao et al. of our group reported the experimental measurements of field emission from an individual single-layer graphene, revealing the correlation between the unique field emission characteristics and the electronic property of a single layer graphene [19]. Yamaguchi et al. reported multiple electron beams from atomically thin edges of reduced graphene oxide (rGO), which presented low threshold field and coherent electron emission as a linear electron source [20]. Other electron emission behaviors from one-atom-thick grapheme surfaces, such as phonon-assisted electron emission [21] and thermionic emission [22], were also studied recently.

All these reported studies have pointed out that the edges of the single-layer graphene or/and FLG play a key role in field emission. This has led us to consider how one may use this edge effect to enhance field emission performance of a graphene films by creating its topographic structures with more edges in favor of field emission. In this study, we have shown that this is possible, through a detailed investigation into the correlation between topographic structures and local field emission characteristics of graphene-sheet films deposited by EPD [5], using micro anode-probe equipped in SEM system.

2. Experimental

The graphene sheets were obtained by chemical exfoliation of artificial graphite, then dispersed into isopropyl alcohol by sonication for 1 h, and deposited on the conductive indium tin oxide (ITO) glass (2 cm × 4 cm), using the EPD method. The concentration of the graphene suspension is 0.1 mg/mL, which consist of up to 80% single-layer graphene. The decorating ion on graphene is Mg^{2+}, which renders the graphene sheets positively charged. The distance between the two electrodes was 5 mm, and the applied voltage was 100–160 V.

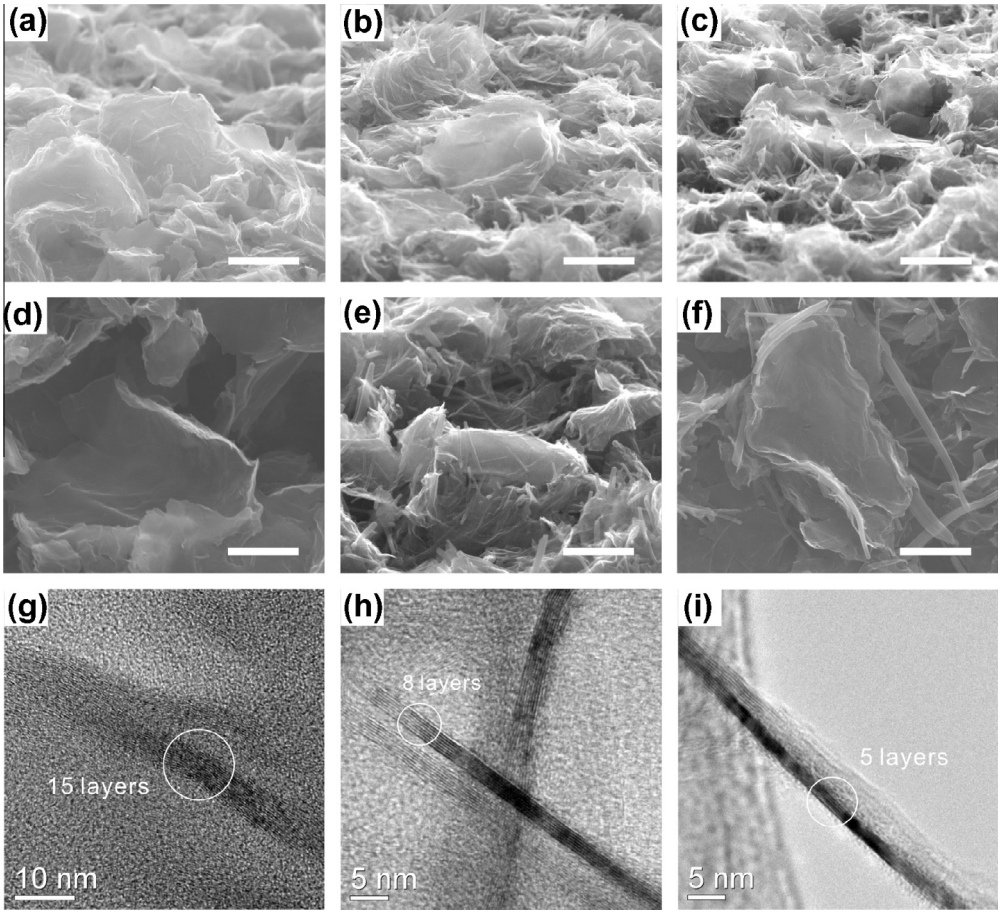

Fig. 1 – High-magnification SEM (a–f) images of the topographic structures of the graphene-sheet films with different deposition time, and the corresponding TEM (g–i) images. (a, d, g) 30 s; (b, e, h) 60 s; (c, f, i) 90 s. The scale bar in (a–c) is 5 μm; the scale bar in (d–f) is 2 μm.

Three tested samples were prepared by setting the deposition time to 30, 60, and 90 s. SEM images of each sample were taken to characterize the morphology differences. HRTEM images were also used to characterize the number of layers of dispersed graphene sheet in each sample, which was scraped onto the surface of TEM grid with 85 μm apertures. To make sure that the observed graphene sheet is mainly from the surface of sample, the grid is placed on the sample, and be softly press the grid to make the upper graphene sheets adhering on the grid.

The local electrical property and field emission measurement on each sample was conducted in a SEM (JEOL JSM-6380LA) chamber equipped with a tungsten tip with a radius of ~1 μm as micro anode-probe. The applied voltage and corresponding current was recorded by a picoammeter with a power supply (Keithley 6487).

3. Results and discussion

Our samples are the films consisting of graphene sheets, thus called graphene-sheet films. The graphene sheets used in this study were obtained by chemical exfoliation of artificial graphite. [4] By changing the deposition time, the topographic structures of graphene-sheet film varies. Fig. 1a–f show typical high-magnification SEM (FEI Quanta 400) images of three samples of graphene-sheet film with deposition times of 30, 60, and 90 s, respectively. One may see that, the randomly oriented graphene sheets exhibit sharp edges. Notably, with 30 s deposition time, the density of the edges of graphene sheet is relatively low and the length of graphene sheet is large. When the deposition time increases, the density of the edges becomes higher and the length of graphene sheet becomes short in the surface layer of the graphene-sheet film. The thickness of graphene sheet film also linearly increases with deposition time as shown in Table 1. The corresponding HRTEM (Joel 2010) images are shown in Fig. 1g and h. The number of layers of dispersed graphene sheet can be clearly seen at the folded edges. We characterized HRTEM images of five typical graphene sheets from each sample. The typical graphene sheet in 30 s sample has about 15–30 layers. While in the 60 and 90 s samples, fewer layer graphene sheets were found existing on the surface of the films, with the number of layers decreased to 8 and 5, respectively. The graphene single-sheet is formed by a number of single-layer graphene with spacing between them being 0.34 nm, in consistent with the generally acknowledged thickness of a single graphene layer. The above results clearly show that with increasing deposition time, thinner and shorter-length graphene sheets will be deposited on the surface of the graphene-sheet film.

Fig. 2a illustrates the basic experimental set-up. A self-made micro anode-probe was equipped within the SEM chamber (SEM, JEOL JSM-6380LA) controlled through a micromanipulator, for *in situ* measurements of different local areas of the surface of graphene-sheet films. The micro anode-probe is a tungsten microtip (~1 μm in radius) made by electrochemical etching. The current–voltage (*I*–*V*) characteristics were recorded by a picoammeter with voltage source (Keithley 6487). Fig. 2b gives the typical SEM image showing how the micro anode-probe is set for field emission measurements of a local area. First, the micro anode-probe was controlled to make contact with the testing area, then the micro anode-probe was moved to a position several micrometers away from the graphene edges along the horizontal direction, thus the interelectrode distance can be directly determined from the SEM image. During the measurements, the electron beam of SEM was systematically blank out. A preconditioning process under low current emission was carried out. We selected five typical spots of each sample to measure their local elec-

Table 1 – Comparison of thickness, length and layers of graphene-sheet films with deposition time of 30, 60, and 90 s.

Deposition time (s)	Thickness (μm)	Length (μm)	Number of graphene layers
30	8.9	>5	15
60	17.5	1–5	8
90	26.3	1–5	5

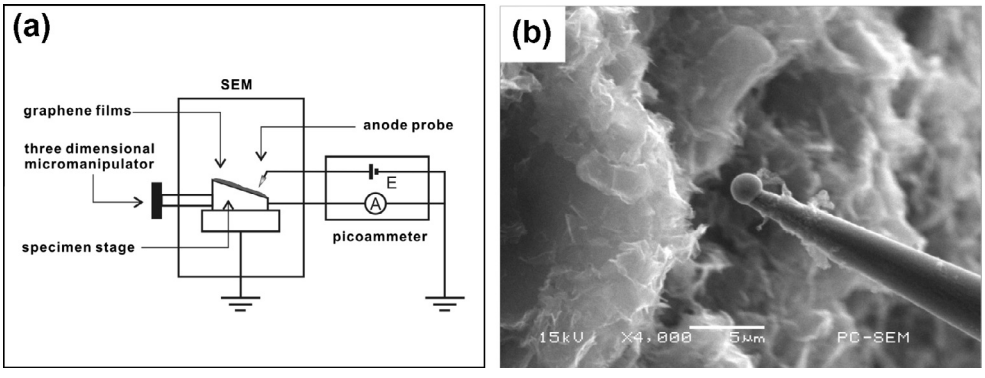

Fig. 2 – (a) Diagram of the basic experimental setup by using micro anode-probe equipped within SEM chamber. (b) SEM images of nanostructures of the graphene-sheet film and the micro anode-probe for field emission tests.

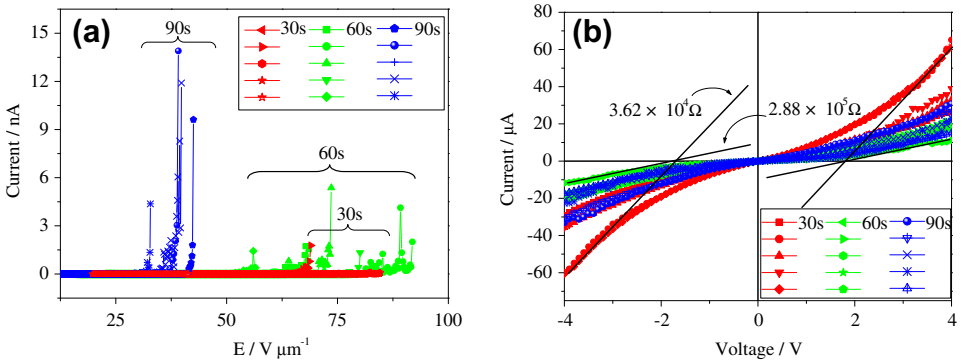

Fig. 3 – (a) Field emission current-applied field (*I–E*) curves, and (b) electrical current-voltage (*I–V*) curves of five selected typical spots from each sample, with deposition time of 30, 60, and 90 s, respectively.

tron-field-emission characteristics before vacuum breakdown, in order to have a more convincing result from a statistic point of view.

Fig. 3a shows the field emission currents (I) of graphene-sheet films as a function of applied electric field (E). We define the turn-on field (E_{to}) as the electrical field needed to produce a current density of 10 μA cm^{-2} and threshold field (E_{th}) as the electrical field needed to produce a current density of 1 mA cm^{-2}. Statistical data on each group of sample spots shows that, the turn-on field and threshold field of 90 s sample (E_{to}, average 32.0 V μm^{-1}, E_{th}, average 33.9 V μm^{-1}) are substantially lower than that of 60s (E_{to}, average 61.1 V μm^{-1}, E_{th}, average 63.6 V μm^{-1}) and that of 30s sample (E_{to}, average 63.3 V μm^{-1}, E_{th}, average 65.6 V μm^{-1}). Also the maximum emission current obtained before vacuum breakdown (I_{max}) of 90 s sample (I_{max}, average 7.89 nA) are substantially larger than that of 60 s (I_{max}, average 2.80 nA) and that of 30 s sample (I_{max}, average 0.42 nA). As may be seen below, these significant differences in field emission characteristics among these samples may be related to the increase of density of graphene edges with increasing deposition time, and the decrease of the thickness of graphene sheets.

The electrical property test was also performed, simply by moving the micro anode-probe to make firm contact with the surface of the graphene-sheet film and applying a voltage sweep from −4 to 4 V. The electrical current–voltage (*I–V*) curves of graphene-sheet films were shown in Fig. 3b, also by selecting five typical spots of each sample. All *I–V* curves exhibit nonlinear behavior in the low voltage region, because ITO glass substrate is an *n*-type oxide semiconductor, which makes the graphene-substrate junction a Schottky-contact. [23,24] We calculated the resistances from the liner section of the *I–V* curves. The resistances of 30 s sample (average 0.07 MΩ) are lower than those of 60 s (average 0.16 MΩ) and 90 s (average 0.13 MΩ). We supposed that because the film thickness of 30 s sample was much thinner than other two samples, we actually measured mainly the contact resistance. All the samples show excellent contact conductance, and the little difference in resistance may not be the pivotal part to affect the field emission performance.

In order to elucidate the underlying physics, we carried out further analysis of the field emission *I–E* data. Often, the *I–E* data are simply interpreted by using the well-known Fowler–Nordheim (FN) plot as below: [3,5,6,10,11,17]

$$I(E) \sim E^2 \exp\left(-\frac{b\varphi_K^{3/2}}{\beta E}\right), \quad (1)$$

where $b = 6.83\ \mathrm{eV}^{-3/2}\,\mathrm{V\,nm}^{-1}$, $\varphi_K \sim \varphi$ (work function $\varphi = 4.7$ eV) and β is the field enhancement factor.

However, in our previous study, we have derived theoretical *I–E* equations, specifically for two-dimensional single-layer graphene, revealing that the field emission process from single-layer graphene may undergo from a low- to high-field transition, which is different from the conventional FN theory [19]. In the high-field regime, the *I–E* relation can be expressed as below:

$$I_H(E) \sim E^{3/2} \exp\left(-\frac{b\varphi_K^{3/2}}{\beta E}\right), \quad (2)$$

and in the low-field regime, the *I–E* relation follows the expression below:

$$I_W(E) \sim E^3 \exp\left(-\frac{b\varphi_K^{3/2}}{\kappa\beta^2 E^2}\right), \quad (3)$$

where κ is the parameter depending on the field penetration depth r and the tight-binding band structure of the graphene. In our calculation, we estimate $\kappa = 0.78r^2/(\mathrm{nm\ V})$ and $r = 3.9$ nm by using the graphene parameters.

Here, we plotted the *I–E* data in coordinates: $\ln(I/E^x) \sim 1/E^y$, where $(x,y) = (2,1)$ for Eq. (1), and $(x,y) = (3/2,1)$ for Eq. (2) and $(x,y) = (3,2)$ for Eq. (3), as shown in Fig. 4a–c, respectively. Because the fluctuation of emission current in some chosen spots may be large, here we picked one typical spot with smooth curve from each sample and calculated their field enhancement factor β based on each equation to see which they can fit into. Fig. 4d shows the β values obtained by different equations; obviously it increases with the increasing deposition time. From the above results, it is found that the $\ln(I/E^x) \sim 1/E^y$ curves in all cases exhibit linear behavior and distinct from the up-bending feature that single-layer graphene has, which we reported earlier [19]. Also the β value of FN plots is almost identical to that of the high-field theory, but both much higher than that of the weak-field theory. It is worth noting that the weak-field theory takes the unique energy band structure of single-layer graphene into account, using the fact that the density of state is linear in the vicinity of the *K* point, and therefore Eq. (3) was deduced. While in the present case, a graphene sheet consists of a few layers of sin-

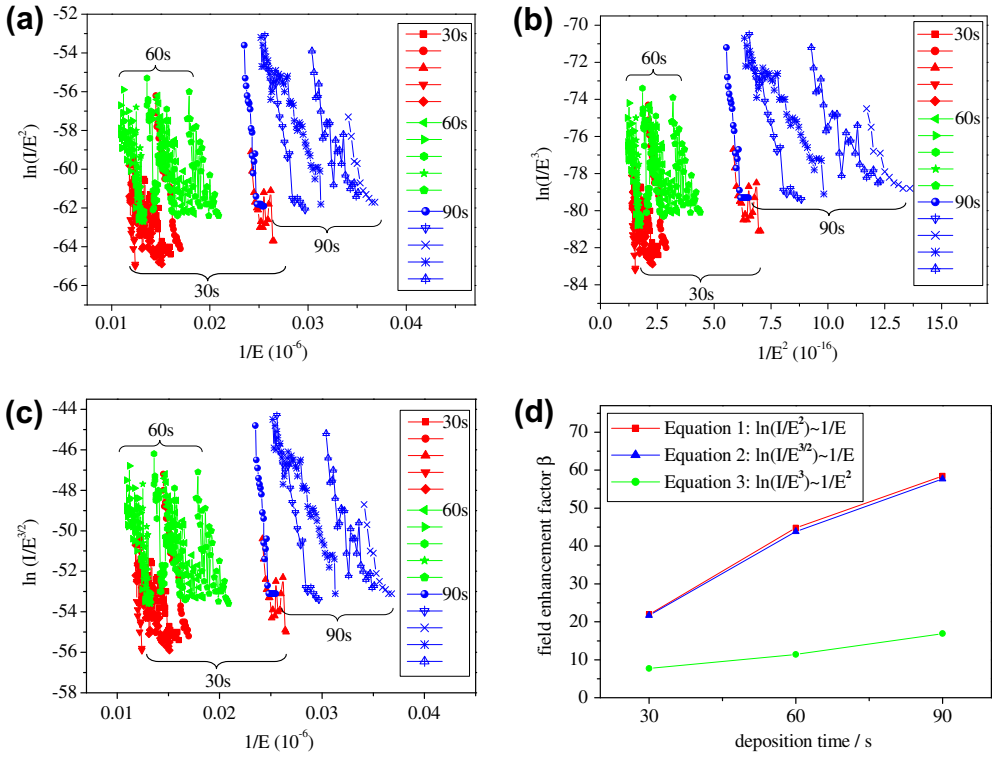

Fig. 4 – (a) Curves in $\ln(I/E^2) \sim 1/E$ coordinate for FN theory. (b) Curves in $\ln(I/E^3) \sim 1/E^2$ coordinate for weak-field regime theory. (c) Curves in $\ln(I/E^{3/2}) \sim 1/E$ coordinate for high-field regime theory. (d) Calculated typical field enhancement factor β based on Eqs. (1)–(3). All curves in this figure correspond to all the *I–E* curves in Fig. 3a.

gle graphene. So the energy band structure of the graphene sheet studied in this paper is different from that of a single-layer graphene, and it should exhibit a collective behavior of several numbers of layers. Thus, in theory the weak-field theory on single-layer graphene is not applicable to our experimental results. The result of the comparison of β values shown in Fig. 4d indicates that the conventional FN theory can be applied to the analysis of the field emission characteristics of the samples of the present study.

Table 2 gives a summary of main results of topographic structures, local electrical and field emission properties of the samples of different deposition time. Here, the emission area *S* was considered to be equal to the area of πr^2, where *r* is the curvature radius of the micro anode-probe. Thus, the maximum current density J_{max} was obtained by I_{max}/S. From the results presented above, we may see that the longer the deposition, the larger emission current is obtained. This may mainly be attributed to the increasing density of graphene sheets as field emitters. Moreover, the longer the deposition, the larger the β value (thus, the higher the local field enhancement), and the lower the turn-on and threshold fields. This may mainly be attributed to the geometrical field enhancement of graphene sheets.

In order to further confirm that the larger β value results from the geometrical field enhancement, we studied the dependence of the field enhancement factor β on the distance between the surface of graphene-sheet films and the micro anode-probe, as denoted by *d*. One may know, as predicted by the classical electromagnetism, the field enhancement will increase with increasing vacuum gap spacing between anode and cathode [25,26]. The previous studies had shown that the $\beta \sim d$ relationship of single CNT may be different, for example, exhibiting asymptotic [25], linear [26] curves, due to the complication of measurement environments and the sample conditions. In our experimental setup, the micro anode-probe (~1 μm in radius) can be considered as a flat electrode, comparing to the size of graphene sheet edge. The field emission measurement of typical spots from a 60 s and a 90 s sample were performed by changing the distance *d*. The corresponding field enhancement factor β was calculated based on FN

Table 2 – Comparison on typical topographic structures, local electrical and field emission characteristics of graphene-sheet films with deposition time of 30, 60, and 90 s.

Deposition time of graphene (s)	E_{to} (V μm^{-1})	E_{th} (V μm^{-1})	I_{max} (nA)	J_{max} (mA cm^{-2})	Resistance (MΩ)	β[a]
30	63.3	65.6	0.42	16.51	0.07	21.94
60	61.1	63.6	2.80	116.82	0.16	44.77
90	32.0	33.9	7.89	440.88	0.13	58.46

[a] β Is calculated based on FN law.

theory and plotted as a function of d in Fig. 5a. A linear relationship is obtained for the curves of both samples. Also the curve for 90 s sample is above the one for 60 s sample, proving that the former has larger geometrical field enhancement.

In order to know why the samples with longer deposition time can have higher β value, theoretical analysis based on field plotting using COMSOL Multiphysics were carried out to find out how the number of layers in a graphene sheet affect the field enhancement factor β. In this study, the single-layer graphene thickness is set to 0.34 nm. The electric potential of graphene layers is set to 0 V and the anode probe is 500 V with an interelectrode distance of 5 μm, based on the present experimental configuration. Thus the macro-field between electrodes E_{macro} is set to 10^8 V/m. The maximum field strength value E_{max} at the emitting surface often at the corner of the sheet, which represents the effective field, was obtained from the simulated local field distribution. Here β values were calculated from E_{max}/E_{macro}, as the number of graphene layers varies from 1 to 30. The radius of anode probe varies from 10 to 500 nm, in order to eliminate the edge effect of anode probe itself. As one may see from Fig. 5b, β increases drastically with the decreasing number of graphene layers, and approaches a constant value when the radius of anode probe is large enough to be considered as a flat plane. It clearly indicates the thickness of graphene plays a key role in the field enhancement. In comparison with experiment, the anode probe (~1 μm in radius) was kept to be around 5 μm away from the graphene edges (Fig. 2b), the graphene sheet is normally several micrometers in height, with the number of graphene layers varies from four to several tens (Fig. 1g–i) in different samples. These conditions are consistent with the theoretical ones. Therefore, the theoretical results given here reveal that the fewer the graphene layer in a sheet, the stronger the local field enhancement is. This leads us to see that the samples with longer deposition time can have stronger field enhancement because their graphene sheets have fewer graphene layers.

Finally, we explain why shorter-length graphene sheets appear on the surface of the graphene films deposited with longer time. We will show below that, the micro-scale graphene sheets will be deposited first on the substrate, while the much smaller (ie shorter-length) nano-scale ones are deposited later during the EPD process. Thus, graphene-sheet films deposited in a longer time will have topographic structures with shorter-length graphene sheets on the surface layer. According to fluid mechanics, the viscosity resistance f of a small object moving through a strong viscous fluid at relatively slow speeds (with low Reynolds number), is proportional to the moving velocity, the square root of cross-section area, and the viscosity coefficient [27]. Here, we assume that the graphene sheet is a cuboid with lateral-surface area (S_1) much larger than cross-section area (S_0). During the EPD process, if the lateral-surface of graphene sheet is parallel to the direction of electric field E (Fig. 6a), the electric field force F and viscosity resistance f can be expressed as below:

$$F = \sigma S_1 E, \tag{4}$$

$$f = -k\eta\sqrt{S_0}v, \tag{5}$$

where σ is the electric quantity per unit area of graphene, k is the related constant, η is the viscosity coefficient related to the fluid properties and temperature, and v is the moving velocity.

When the lateral-surface of graphene sheet parallel to E arrives at the uniform motion state ($F = f$), the maximum velocity of the graphene sheet can be written as follows:

$$v_{max//} = \frac{\sigma E S_1}{k\eta\sqrt{S_0}} \tag{6}$$

Hypothetically the micro-scale graphene is 100 times larger than the nano-scale graphene in every dimension, and then its maximum velocity will be 100 times larger than that of nano-scale graphene sheet, according to the calculated results based on Eq. (6).

Similarly, if the lateral-surface of graphene sheet is perpendicular to the direction of electric field E (Fig. 6b), the maximum velocity of graphene can be written as below:

$$v_{max\perp} = \frac{\sigma E\sqrt{S_1}}{k\eta}, \tag{7}$$

which is proportional to the square root of lateral-surface area. In this case, if the micro-scale graphene is 100 times lar-

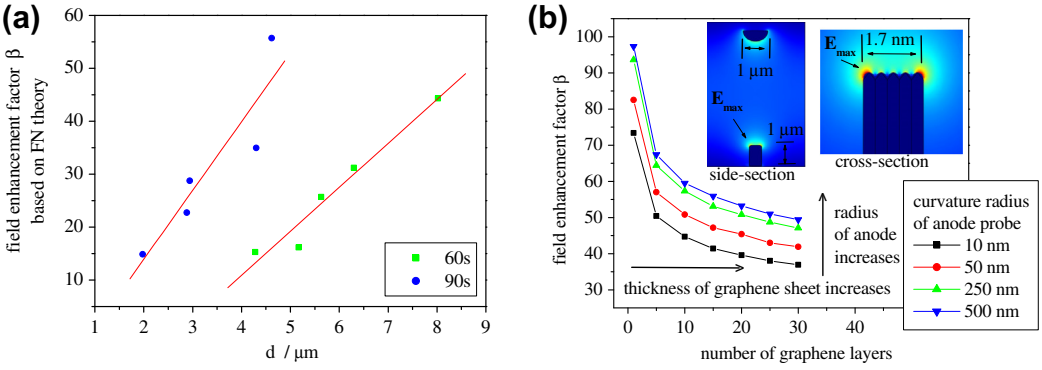

Fig. 5 – (a) Calculated $\beta \sim d$ relationship of 60 and 90 s sample. (b) Numeric simulation for the dependence of field enhancement factor β on the number of graphene layers and curvature radius of the micro anode-probe. Inset: local field distribution of a 5-layer graphene sheet (side-section and cross-section view, 1 μm in height, 0.5 μm in width, and 1.7 nm in thickness) with the curvature radius of the micro anode-probe being 500 nm, showing that the edge of graphene sheet has the maximum electric field strength E_{max}.

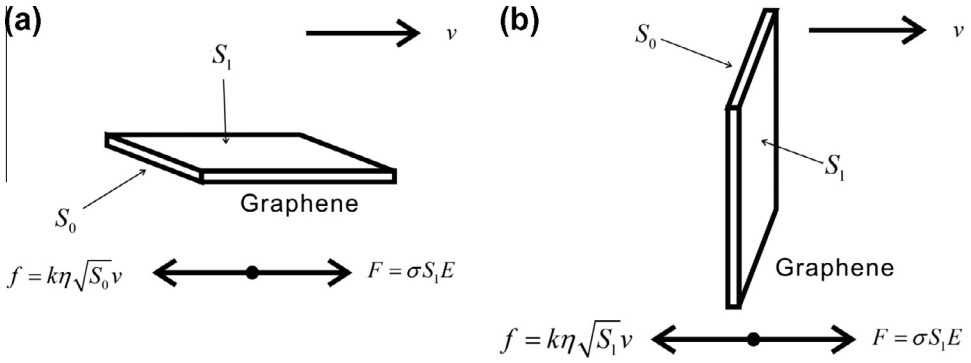

Fig. 6 – Scheme of the force analysis of a graphene sheet in different situation: (a) with its lateral-surface parallel to the electric field and (b) with its lateral-surface perpendicular to the electric field during EPD process.

ger than the nano-scale graphene in every dimension, then its maximum velocity will be 100 times larger than that of nano-scale graphene sheet, according to the calculated results based on Eq. (7).

Therefore, we have reached a conclusion in both situations (Fig. 6a and b) that larger-scale graphene sheets have a faster deposition rate in EPD process. Thus they are deposited first. With increasing deposition time, the small-scale graphene sheets arrive. Thus, graphene film samples used in this study have different topographic structures; the sample with 30 s deposition time has larger graphene sheets in the surface layer, and the one with 90 s has smaller graphene sheets. This explains how the different topographic structures are formed with variation of deposition time.

4. Conclusions

EPD is a valuable method for graphene-sheet film deposition, and we have found that field emission performance from graphene-sheet films prepared by EPD can be enhanced by optimizing deposition time. Our experimental studies have shown that samples prepared with longer deposition time have better field emission performance. SEM images show that the topographic structure of the surface layer of our samples deposited with longer time is formed with smaller-size (thus shorter-length) graphene sheets, in comparison with those with shorter deposition times. Further HRTEM images reveal that these shorter-length sheets have fewer graphene layers in a sheet. These shorter-length and thinner graphene sheets can give rise to geometrical field enhancement, and thus result in the lower turn-on and threshold fields, as found both experimentally and theoretically. We have finally explained theoretically why these smaller-size graphene sheets deposit on the surface layer of samples with longer deposition time in an EPD process.

Acknowledgements

The authors gratefully acknowledge the financial support of the project from the National Key Basic Research Program of China (Grant No. 2013CB933601 and 2010CB327703), the National Natural Science Foundation of China (Grant No.U1134006, 50725206, 51102287 and 51290271), the Science and Technology Department of Guangdong Province, the Economic and Information Industry Commission of Guangdong Province, and the Science & Technology and Information Department of Guangzhou City.

REFERENCES

[1] Novoselov KS, Geim AK, Morozov SV, Jiang D, Zhang Y, Dubonos SV, et al. Electric field effect in atomically thin carbon films. Science 2004;306:666–9.
[2] Geim AK, Novoselov KS. The rise of graphene. Nat Mater 2007;6:183–91.
[3] Zhu Y, Murali S, Cai W, Li X, Suk JW, Potts JR, et al. Graphene and graphene oxide: synthesis, properties, and applications. Adv Mater 2010;22:3906–24.
[4] Wu ZS, Ren W, Gao L, Liu B, Jiang C, Cheng HM. Synthesis of high-quality graphene with a pre-determined number of layers. Carbon 2009;47:493–9.
[5] Wu ZS, Pei S, Ren W, Tang D, Gao L, Liu B, et al. Field emission of single-layer graphene films prepared by electrophoretic deposition. Adv Mater 2009;21:1756–60.
[6] Qi JL, Wang X, Zheng WT, Tian HW, Hu CQ, Peng YS. Ar plasma treatment on few layer graphene sheets for enhancing their field emission properties. J Phys D Appl Phys 2010;43:055302-1–6.
[7] Li J, Chen J, Shen B, Yan X, Xue Q. Temperature dependence of the field emission from the few-layer graphene film. Appl Phys Lett 2011;99:163103-1–3.
[8] Soin N, Roy SS, Roy S, Hazra KS, Misra DS, Lim TH, et al. Enhanced and stable field emission from in situ nitrogen-doped few-layered graphene nanoflakes. J Phys Chem C 2011;115:5366–72.
[9] Teii K, Nakashima M. Synthesis and field emission properties of nanocrystalline diamond/carbon nanowall composite films. Appl Phys Lett 2010;96:023112-1–3.
[10] Qian M, Feng T, Ding H, Lin L, Li H, Chen Y, et al. Electron field emission from screen-printed graphene films. Nanotechnology 2009;20:425702-1–6.
[11] Lu Z, Wang W, Ma X, Yao N, Zhang L, Zhang B. The field emission properties of graphene aggregates films deposited on Fe–Cr–Ni alloy substrates. J Nanomater 2010;2010:148596-1–4.
[12] Goswami S, Maiti UN, Maiti S, Nandy S, Mitra MK, Chattopadhyay KK. Preparation of graphene–polyaniline composites by simple chemical procedure and its improved field emission properties. Carbon 2011;49:2245–52.

[13] Das S, Seelaboyina R, Verma V, Lahiri I, Hwang JY, Banerjee R, et al. Synthesis and characterization of self-organized multilayered graphene–carbon nanotube hybrid films. J Mater Chem 2011;21:7289–95.
[14] Hwang JO, Lee DH, Kim JY, Han TH, Kim BH, Park M, et al. Vertical ZnO nanowires/graphene hybrids for transparent and flexible field emission. J Mater Chem 2011;21:3432–7.
[15] Lahiri I, Verma VP, Choi W. An all-graphene based transparent and flexible field emission device. Carbon 2011;49:1614–9.
[16] Lee DH, Lee JA, Lee WJ, Kim SO. Flexible field emission of nitrogen-doped carbon nanotubes/reduced graphene hybrid films. Small 2011;7(1):95–100.
[17] Lee SW, Lee SS, Yang EH. A study on field emission characteristics of planar graphene layers obtained from a highly oriented pyrolyzed graphite block. Nanoscale Res Lett 2009;4:1218–21.
[18] Wang HM, Zheng Z, Wang YY, Qiu JJ, Guo ZB, Shen ZX, et al. Fabrication of graphene nanogap with crystallographically matching edges and its electron emission properties. Appl Phys Lett 2010;96:023106-1–3.
[19] Xiao ZM, She JC, Deng SZ, Tang ZK, Li ZB, Lu JM, et al. Field electron emission characteristics and physical mechanism of individual single-layer graphene. ACS Nano 2010;4(11):6332–6.
[20] Yamaguchi H, Murakami K, Eda G, Fujita T, Guan P, Wang W, et al. Field emission from atomically thin edges of reduced graphene oxide. ACS Nano 2011;5(6):4945–52.
[21] Wei X, Golberg D, Chen Q, Bando Y, Peng L. Phonon-assisted electron emission from individual carbon nanotubes. Nano Lett 2011;11:734–9.
[22] Wei X, Bando Y, Golberg D. Electron emission from individual graphene nanoribbons driven by internal electric field. ACS Nano 2012;6(1):705–11.
[23] Zhang Z, Yao K, Liu Y, Jin C, Liang X, Chen Q, et al. Quantitative analysis of current–voltage characteristics of semiconducting nanowires: decoupling of contact effects. Adv Funct Mater 2007;17:2478–89.
[24] Chen JB, Xu CJ, She JC, Deng SZ, Chen J, Xu NS. Pulsed-laser treatment of solution-grown ZnO nanowires in nitrogen: Enhancing in electrical conduction and field emission. J Appl Phys 2010;107:024312-1–6.
[25] Bonard JM, Dean KA, Coll BF, Klinke C. Field emission of individual carbon nanotubes in the scanning electron microscope. Phys Rev Lett 2002;89(19):197602-1–4.
[26] Xu Z, Bai XD, Wang EG. Geometrical enhancement of field emission of individual nanotubes studied by in situ transmission electron microscopy. Appl Phys Lett 2006;88:133107-1–3.
[27] Batchelor GK. An introduction to fluid dynamics. Cambridge: Cambridge University Press; 2005.